Title: Petrographical evidence of the >1000 km voyage of a white pumice raft that arrived at the Ogasawara and Nansei Islands after the October 2023 earthquakes in the southern Izu Islands

Kenta K., Yoshida[1], Reona Hiramine[2,3], Daisuke Ishimura[3], Tomoki Sato[1], Yu Maruya[4]

1 Research Institute for Marine Geodynamics, Japan Agency for Marine-Earth Science and Technology, Natsushima-cho 2-15, Yokosuka, Kanagawa, 237-0061 Japan

2 Research Department, National Museum of Japanese History, Sakura, 285-0017 Japan

3 Department of Geography, Tokyo Metropolitan University, Hachioji, 192-0397 Japan

4 Necono-Wakuwaku Nature School, Toma 822-1, Nakagamigun Nakagusukuson, Okinawa, 901-2406 Japan

Corresponding author: Kenta K. Yoshida, yoshida_ken@jamstec.go.jp, +81-46-867-9782

Abstract:

An earthquake swarm occurred at Sofu Seamount near Izu-Torishima in the Izu-Ogasawara (Bonin) Arc, Japan, on 8 October 2023, followed by the arrival of unexpectedly-large tsunamis over a wide area of the Pacific coast of southwest Japan. On 20 October, aerial observation identified floating pumice rafts extending for ~80 km in the area the seamount, which were subsequently sampled and found to comprise white-colored rhyolitic pumice containing dark-colored patches. Subsequently, in the summer and autumn of 2024, white pumice, which can be clearly distinguished from the pre-existing gray and black pumice from recent eruptions of oceanic volcanoes, was stranded on the coasts of the Nansei and Izu-Ogasawara Islands. This study presented petrographic and geochemical characteristics of the white drift pumice to investigate the dispersal of the small scale pumice rafting.

White pumice clasts were collected at Okinawa (Nansei Islands) and Hahajima (Ogasawara Islands), and found to have the same petrographic and geochemical characteristics. The clasts consist of microlite-free white pumice with fine vesicles and gray-colored frothy patches, similar to the clasts collected immediately after the earthquake swarm at Sofu Seamount in October 2023. In addition, the clasts contain black enclaves containing Mg-rich olivine and clinopyroxene, and Ca-rich plagioclase. Although the white pumice clasts collected at similar times included those with different characteristics, the finding of the same pumice type over a distance of >1000 km suggests that the pumice clasts drifted over a wide area despite the small size of the pumice rafts.

Keywords: drift pumice, Izu-Ogasawara Arc, submarine volcano, mafic enclave

Introduction

Pumice is a porous volcanic product that is commonly formed by explosive eruptions of silicic to intermediate magma. Due to its high porosity, pumice commonly floats on water and is transported to distant locations, (i.e., pumice rafting; Bryan et al., 2004, 2012, Hiramine et al., 2023). Large-scale pumice rafting can lead to the dispersal of marine species (Bryan et al., 2004, 2012), gravelling of coastal environments (Ohno et al., 2022), and obstruction of marine traffic (Maeno et al., 2022).

A large-scale pumice rafting event occurred in 2021–2022 in the coastal area of Japan, sourced from the 2021 eruption of Fukutoku-Oka-no-Ba (FOB) in the Izu–Ogasawara (Bonin) Arc on 13–15 August 2021 (Maeno et al., 2022; Ohno et al., 2022; Yoshida et al., 2022a, b, c; Takeuchi et al., 2024; Ishimura & Hiramine, 2025). The ejected volume of pumice is estimated to be 0.1–0.4 km^3 (Maeno et al., 2022) and it arrived at most coastal areas in Japan (Yoshida et al., 2022a, c; Ishimura & Hiramine, 2025). Pumice also arrived at Thailand after drifting for >4000 km (Yoshida et al., 2022b).

Another pumice rafting event, which was widely observed in coastal Japan, occurred in 2024 and was sourced from the 2022 and 2023 eruptions of off-Ioto Island, which is located near FOB (Miwa et al., 2024; Nagai et al., 2024; Japan Agency for Marine-Earth Science and Technology, 2024). Although the estimated ejected volume of the 2023 eruption was small (~0.00005 km^3; Nagai et al., 2024), the distinctive black pumice was observed in several areas of Japan, including on both the Pacific and Sea of Japan coasts. Numerical simulations indicate the pumice raft drifted westward from the southern Izu–Ogasawara Arc, which is an area of active submarine volcanoes and volcanic islands (e.g., Tamura et al., 2009, 2023), likely arrive at the Nansei Islands (e.g., Okinawa Island) via the Kuroshio Counter current within 2–6 months of eruption (Tada et al., 2021; Nishikawa et al., 2023). Therefore, the Nansei Islands appears to be a pumice downtown accumulating drift pumice from marine volcanoes in the

western North Pacific (Fig. 1a).

In the area around Sofugan Island in the central Izu–Ogasawara Arc, an earthquake swarm with strong T-waves and corresponding unexpectedly-large tsunamis (up to 0.7 m wave height on Hachijojima Island and smaller height along the Pacific coast of Japan) occurred on 8 October 2023 (UTC) (Mizutani & Melgar, 2023; Fujiwara et al., 2024; Sandanbata et al., 2024; Obana et al., 2025). Based on T-phase wave analysis, the earthquake epicenters were located in the topographic high ~10 km west of Sofugan (Fujiwara et al., 2024), which is the location of Sofu Seamount where no volcanic activity has previously been reported. Fujiwara et al. (2024) and Minami & Tani (2024) detected significant bathymetric changes at the seamount after the earthquake swarm, indicating the earthquakes and tsunamis were generated by volcanism. On 20 October, aerial observations by the Japan Coast Guard identified floating pumice rafts extending for 80 km in a N–S direction (Fig. 1b: Japan Coast Guard, 2023), although remote identification by satellite images was not possible (Kuwatani et al., 2024). Immediately after the aerial observation, the R/V *Keifu Maru* collected white and gray pumice clasts in the areas near Izu–Torishima and Sofugan on 27 October, the latter of which were sourced from FOB (Oikawa et al., 2023). Preliminary geochemical analysis indicated that the white pumice is rhyolite and was sourced from the back-arc rift zone of the Izu–Ogasawara Arc, although the actual source volcano was not constrained (Earthquake Research Institute, Uiversity Tokyo, 2023; Oikawa et al., 2023).

In June 2024, about eight months later, newly stranded white pumice, which is aphyric with fine bubbles and resembles Japanese gluten cakes, was observed on the coasts of Okinawa Island in the Nansei Islands. The stranding of white pumice clasts was also observed at coasts of Okinawa and Ogasawara Islands, mainly during July–September 2024 (Fig. 1a). The petrographic characteristics of the newly obtained white pumice clasts are similar to those of the drift pumice collected immediately after the earthquakes, thereby indicating the wide dispersal of this white pumice, despite the small total volume of the pumice rafts.

This paper describes the petrographic and geochemical characteristics of the white pumice clasts and compares them with the pumice clasts collected immediately after the earthquakes. We also discuss the possible dispersal of small pumice rafts sourced from unknown submarine volcanoes.

Samples and Analytical Methods

We collected white pumice from five localities including Okinawa and islands in the Izu–Ogasawara Arc (Figs. 1a and 2a–f). The pumice clasts appeared to have been newly washed ashore and occurred near the high tide line, although the amount of stranded pumice was not large. Although previously stranded pumice clasts remain on the beaches, including those from the two major pumice rafting events that followed the 2021 eruption of FOB (gray pumice) and 2023 eruption of Ioto (black pumice), the newly stranded white pumice can be readily distinguished based on their color, texture, and shape. The white pumice at Okinawa was recognized in June, 2024, and the amount of stranded pumice increased after August 2024. We also found newly stranded white pumice on the coasts of Chichijima and Hahajima islands in the southern Izu–Ogasawara Arc in July 2024. At Niijima in the northern Izu–Ogasawara Arc, a small amount of white pumice was collected in October 2024. The newly stranded white pumice clasts are subangular as compared with the previous two major pumices stranding events, except for clast OMT-3 that is rounded (Fig. 2e). The largest white pumice clast was found on Okinawa Island and had a long axis of ~20 cm in length (Fig. 2a). However, most pumice clasts were 10 cm in size. We selected representative samples from each locality for analysis (Table 1).

Whole-rock major element compositions were determined by X-ray fluorescence (XRF) spectrometry (Rigaku ZSX Primus II) at the Japan Agency for Marine-Earth Science and Technology (JAMSTEC), Yokosuka, Japan, following the procedures of Tani et al. (2005).

Trace element analysis was undertaken on two selected pumice clasts collected from Hahajima and Okinawa, by solution inductively coupled plasma mass spectrometry (ICP–MS; ThermoFisher Scientific iCAP Qc), using the same procedures as Yoshida et al. (2022a). The reliability of the acquired data was assessed by analysis of a basalt reference material (JB-2: Jochum et al., 2016).

Mineral and glass compositions were determined with a field-emission gun electron microprobe (EMP) analyzer equipped with five wave-length dispersive X-ray detectors (JEOL JXA-8500F) at JAMSTEC. The analytical conditions were 15 kV and 10 nA for the accelerating voltage and beam current, respectively. The beam diameter was set to 3 μm for minerals and 5 μm for glass. However, some glass with fine texture was analyzed with smaller beam diameters down to 3 μm. X_{Mg} values for mafic minerals were calculated as $Mg/(Mg + Fe^{2+})$, and X_{An} values for plagioclase (Pl) were calculated as Ca/(Ca + Na + K).

The mineral species of the SiO_2 phases in some samples were determined by Raman spectroscopy using a Raman spectrophotometer (RAMANtouch VIS-HP-MAST; Nanophoton) equipped with a 532 nm semiconductor green laser at JAMSTEC. The laser power at the sample surface was 1–2 mW, and the data were acquired in 2 × 20 s cycles to eliminate accidental cosmic rays. The spectrometer was calibrated to the 520.7 cm^{-1} peak of a Si wafer.

Whole-rock Geochemistry

In a total alkalis–silica (TAS) classification diagram (Figure 3a), the studied pumice has a rhyolitic composition (SiO_2 = 70.2–72.0 mass%), except for sample OMT-3 that has a dacitic composition (SiO_2 = 67.0 mass%). Sample NJ24-2 has a slightly alkali-rich composition with $Na_2O + K_2O$ = 7.5 mass%, while three samples (KTK-7, NC24-7, and HNU-1) have similar composition to each other, identical to the composition reported for the drift pumice collected near Izu–Torishima in 2023 (Fig. 3a, Oikawa et al., 2023).

Based on petrographic characteristics (see below), samples NC24-7 and KTK-7 were chosen for whole-rock trace element analyses. The two white pumice clasts have almost identical values of Ba/La and La/Sm (~20 and ~2, respectively; Fig. 3c).

Petrography and Mineral/Glass Chemistry

Amongst the five studied pumice clasts, NC24-7 collected from Okinawa Island and KTK-7 collected from Hahajima have similar characteristics, with a relatively massive, white and vesicular matrix (Fig. 2a–c), gray-colored frothy patches that are several millimeters to >4 cm in size (Figs. 2a, and c) and black enclaves up to 1 cm in size (Fig. 2b). The matrix of the pumice consists of microlite-free glass (SiO_2 =77.8 mass%) and contains phenocrysts of clinopyroxene (Cpx), orthopyroxene (Opx), Pl, and magnetite (Mag). The Cpx is augite with X_{Mg} = 0.65–0.78 while the Opx is Fe-rich enstatite with X_{Mg} = 0.56–0.75. The Pl phenocrysts exhibit decrease in Ca contents towards the rim, with X_{An} of up to 0.52 in the cores and X_{An} of 0.32 at the rims. Some grains have antecrystic cores of intermediate Pl with X_{An} = 0.38 and irregular-shaped boundaries (Fig. 4a). The ordinary matrix of the white-colored pumice contains fine vesicles down to <10 μm in size, and the boundary of this matrix with frothy patches comprises coherent large bubbles (Fig. 4b). The mineral assemblage in the frothy patches is the same as that in the ordinary matrix, but the coarse plagioclase in the frothy patches occasionally contains antecrystic core with calcic compositions (X_{An} = 0.81: Fig. 4c). The groundmass glass in the frothy patches has slightly lower SiO_2 contents (SiO_2 = 76.2 mass%) as compared with the ordinary matrix of the pumice (Fig. 3b). The black enclaves are characterized by single or multiple phenocrysts surrounded by a microlite-rich rind (Fig. 4d). The phenocrysts in the black enclave are olivine (Ol, X_{Mg} = 0.77), Mg-rich Cpx (X_{Mg} = 0.82), and calcic Pl (X_{An} = 0.90). The vesicles in the microlite-rich matrix occasionally contain diktytaxitic cristobalite (Crs) (Fig. 4e). Rare melt inclusions occur in Cpx, with daughter mineral phases that are possibly

amphibole and opaque minerals. The residual glass in the melt inclusions is SiO_2-poor (SiO_2 ~63 mass%) (Fig. 4f).

Sample HNU-1 collected from Chichijima a relatively massive, white vesicular matrix (Fig. 2d). Phenocrysts are Cpx (X_{Mg} = 0.78), Opx (X_{Mg} = 0.61), intermediate Pl with Ca-rich cores (X_{An} = 0.51) and Ca-poor rims (X_{An} = 0.34), Mag, and quartz (Qz) (Fig. 4g). Magnesium-rich Cpx (X_{Mg} = 0.90) and calcic Pl (X_{An} = 0.92) xenocrysts are occasionally present and surrounded by a microlite-rich rind that contains olivine (X_{Mg} = 0.69) (Figs. 4i–j). The groundmass glass has SiO_2 = 76.5 mass%, whereas the melt inclusion in the xenocrystic Cpx have SiO_2 = 64 mass%.

Sample OMT-3 (Fig. 2e) collected from Hahajima contains coarse vesicles (mostly >100 μm) and consists of phenocrysts of Cpx (X_{Mg} = 0.86), Opx (X_{Mg} = 0.60), Pl (X_{An} = 0.40), Ol (X_{Mg} = 0.75), Mag, and ilmenite (Ilm) in a groundmass of microlite-free glass (Fig. 4k). Dark-colored mineral aggregates of up to 1 cm in size consist of Ca-rich Pl (X_{An} = 0.63), Cpx (X_{Mg} = 0.82), Opx (X_{Mg} = 0.75), Ol (X_{Mg} = 0.71), Mag, and weakly vesiculated glass (Fig. 4l). The groundmass glass in the pumice matrix has SiO_2 = 76.5 mass%, whereas the glass in the dark-colored aggregate has SiO_2 = 74 mass%.

Sample NJ24-2 was collected from Niijima and has a texture with elongated vesicles (Fig. 2f). The phenocryst minerals are Cpx (X_{Mg} = 0.44), Opx (X_{Mg} = 0.35), Pl (X_{An} = 0.35), Ol (X_{Mg} = 0.23), and Mag, with the groundmass glass having SiO_2 = 72 mass% (Fig. 4m).

Discussion and Implications

Based on the whole-rock geochemistry and petrographic characteristics, samples NC24-7 and KTK-7, from Okinawa and Hahajima, respectively, are considered to have the same origin. The trace element characteristics of the studied pumice is also compared with silicic rocks from other volcanoes in the Izu–Ogasawara Arc (Tamura et al., 2009). The studied pumice clasts,

along with the white pumice collected near Izu–Torishima have Ba/La = ~20 which can be distinguished from the rocks from the volcanic front of the Izu-Ogasawara Arc (Fig. 3c). La/Sm ~2 is clearly different from that of the drift pumice from Fukutoku-Oka-no-Ba which is commonly observed in the Japanese coastal area (Yoshida et al., 2022a). Oikawa et al. (2023) reported that these geochemical characteristics are typical of those of volcanic rocks from the back-arc rift of the Izu–Ogasawara Arc. Although the timing of the stranding of clast KTK-7 is not clear, it is likely that the white pumice observed near Izu–Torishima drifted southward and arrived at the Ogasawara Islands, and subsequently drifted westward in the Kuroshio Counter current and arrived at the Nansei Islands like other drift pumice clasts from the Ogasawara Islands (Yoshida et al., 2022a). Given that xenocrystic mafic minerals and corresponding dacitic melt inclusions are observed, sample HNU-1 collected from Chichijima could also have a similar origin, although it has slightly different macroscopic characteristics. In contrast, sample OMT-3 has a different mineral assemblage (e.g., phenocrystic olivine) and a SiO_2-poor dacitic whole-rock composition. Sample NJ24-2 has different characteristics from above four samples including the presence of Fe-rich minerals, which occasionally occurs in some rhyolitic eruptions (e.g., Grebennikov & Maksimov, 2006).

Given that drift pumice can float for several years (e.g., Bryan et al., 2012; Takeuchi et al., 2024; Ishimura & Hiramine, 2025), a stranded pumice deposit can contain clasts derived from different volcanoes and eruptions (Hiramine et al., 2023). Mori et al. (1992) reported substantial pumice stranding on the coast of Hiratsuka the southern Kanto area after the passage of a typhoon in the autumn of 1991. These pumice clasts had similar characteristics to the pumice sourced from FOB, indicating that pumice ejected from the 1986 eruption had once been stranded and then underwent renewed drift five years after the eruption. Extreme storms, such as typhoons, can be responsible for the transportation of light materials, such as plastic debris, from land to sea (Nakajima et al., 2022) which is also applicable for pumice transportation. Aoki et al. (2022) reported a small amount of pumice stranded at Izu–Oshima in

220 the Izu Islands in November 2021 that coincided with the large-scale pumice rafting event from
221 FOB, but the former different mineral and glass compositions as compared with the pumice
222 from FOB. Given that sample NJ24-2 collected from Niijima had different origin from other
223 studied samples, its petrographic and geochemical features should be confirmed to identify the
224 drift pumice dispersal. As such, identifying the origin(s) of small pumice rafting event is
225 challenging. In the case of the 2021 FOB eruption, the amount of drift pumice was large enough
226 (i.e., a pumice raft of 0.1-0.4 km^3 corresponding to VEI = 4; Maeno et al., 2022) to easily
227 identify its arrival at several sites in Japan elsewhere (Yoshida et al., 2022a, b, c; Ishimura &
228 Hiramine, 2025). However, more-recent pumice rafting events from the Izu–Ogasawara Arc to
229 coastal Japan, which involve drift of >1000 km, include the 2023 eruption of Ioto volcano
230 (Japan Agency for Marine-Earth Science and Technology, 2024). The 2023 Ioto eruption was
231 small in scale and the total ejected volume was estimated to be ~0.00005 km^3 (VEI = 1) (Nagai
232 et al., 2024), although distinctive black pumice clasts were first observed at Okinawa and
233 subsequently at several coastal areas of Japan within six months of the eruption (Japan Agency
234 for Marine-Earth Science and Technology, 2024). This indicates that small-scale pumice rafting
235 from a small eruption can be detected even if the drift distance is >1000 km.
236 Oikawa et al. (2023) reported on the appearance and geochemical characteristics of
237 drift pumice clasts collected near Izu–Torishima in October 2023 (Fig. 1b). Although detailed
238 petrographic information, such as mineral chemistry, is not available for these clasts, their
239 whole-rock major and trace element characteristics are similar to those of samples NC24-7 and
240 KTK-7 (Fig. 3a and c). Oikawa et al. (2023) also identified Pl-bearing dark-colored enclaves
241 with a porphyritic texture, which appear to correspond to the frothy patches in the pumice clasts
242 of the present study. In contrast, the black enclaves in the two studied pumice clasts were not
243 identified in the pumice collected near Izu–Torishima. These black enclaves may record
244 information about mafic magma involved in the eruption. Several models have been proposed
245 for mafic enclave formation and related magma mixing (e.g., Coombs et al., 2003; Ohashi et

al., 2024). The mafic enclaves are first injected into silicic magma reservoir, and then crystallization and vapor exsolution occur in the enclaves. Based on the degree of crystallinity of each enclave, the enclave is either mixed with the surrounding magma or solidified. Yoshida et al. (2022a; 2023) reported coexisting black and gray pumice in a single clast of the 2021 eruption of Fukutoku-Oka-no-Ba; however, in their case, no apparent compositional differences were observed among different-color domains, but only significant precipitation of magnetite and biotite nanolites in the black domain was recognized. Yoshida et al. (2023) indicated that the infiltration of oxidizing water in the former-black domain brought nucleation of nanolites to make the pumice black without apparent compositional changes. In the studied samples, the frothy patches, showing slightly lower SiO_2 content, may represent the well-mixed domain, while the black enclaves represent the completely solidified parts. In the vesiculated black enclaves, precipitation of cristobalite from the vapor phase resulted in diktytaxitic texture (Fig. 4e; Sakurai et al., 2024). It is unclear whether the white pumice investigated by Oikawa et al. (2023) contains xenocrysts in the microlite-rich groundmass (i.e., the smallest component in the black enclaves); however, the limited number of pumice clasts studied by Oikawa et al. (2023) may have hindered the identification of such enclaves.

Pumice clasts similar to those observed in October 2023 near Izu–Torishima drifted to Hahajima in the southern Izu–Ogasawara Arc and Okinawa in the Nansei Islands (Fig. 1a), even though the original pumice raft was not large. Although the arrival date on Hahajima is not well determined, the white pumice arrived at Okinawa as early as June 2024, and subsequently considerable amount arrived in August 2024. In the case of the pumice rafting from FOB to Okinawa, the 1986 eruption occurred in January and the first arrival at Okinawa was in the following May, while the 2021 eruption occurred in August and the first arrival was in October of the same year (Yoshida et al., 2022a, c). It is possible that drifting in summer–autumn is faster than in winter–spring. Compared with FOB pumice rafting, pumice drift from the area near Izu–Torishima to Okinawa within eight months (i.e., late October to June in the following

year) appears plausible. Kuwatani et al. (2024) undertook a back-tracking drift simulation, based on wind and ocean current data, to investigate the source of these pumice clasts. The ocean currents in the relevant area and at the appropriate time were mostly southwards, indicating the pumice started drifting from the northern back-arc basin region near Myojinsho and Sumisujima at 3-5 days before its discovery (Fig. 1b). Based on this simulation, Kuwatani et al. (2024) suggested that these pumice clasts were sourced from an unknown small eruption of a submarine volcano that was not recognized by remote observations, such as satellite imaging and seismic monitoring. Although the discovery of the pumice raft coincided with an earthquake swarm at Sofu Seamount on 8 October 2023, the ocean currents at this time are not consistent with this area being the source region. Obana et al. (2025) undertook a seismic analysis immediately after the earthquake swarm during the period from 11 November 11 to 3 December 3 2023, which indicated that the seismic activity occurred not only below the Sofu Seamount, but also in a linear region up to 50 km the north of the seamount (Fig. 1b). They inferred that this was caused by a extensive magmatism in the back-arc rift zone north of the seamount (i.e., the Torishima Rift).

Rashidov et al. (2015) reported on the occurrence of sunken pumice at the Sofu Seamount based on dredge surveys undertaken in 1977 by the Russian R/V *Vulkanolog*, although detailed chemical data are not available for these samples. As such, a direct comparison of the studied sample with the rocks from the Sofu Seamount is not possible. The simulation and seismic observations, along with the pumice geochemical analyses indicate increased magmatic activity in the back-arc rift zone of the Izu–Ogasawara Arc. To further investigate such activities, comprehensive geophysical and geological surveys of the possible source region are required, including sampling.

Acknowledgements

This research was partly supported by the JSPS KAKENHI (JP19K14825, JP19H01999, and JP24K00743 to K.Y.); the Disaster Geography Research Grant from The Association of Japanese Geographers to RH, the Joint Usage and Research Program of the Earthquake Research Institute, the University of Tokyo (ERI JURP 2021-B-01), the Ogasawara Research Committee of Tokyo Metropolitan University, the MEXT Volcano Practical Human Resource Development Support Program Japan (JPJ202414), and the ERCA Environment Research and Technology Development Fund (JPMEERF20244002) from the Ministry of the Environment of Japan. We would like to thank Stallard Scientific for their English language editing. We also thank the children of Necono–Wakuwaku Nature School who helped find and sample the various types of stranded pumice on Okinawa Island.

References

Aoki, K., Hiramine, R., Ishimura, D., Watanabe, T., & Suzuki, T. (2022) Did drifted pumices on the Sanohama beach, the southeastern part of the Izu-Oshima Island derive from the 2021 Fukutoku-Oka-no-Ba eruption, Japan? *Japan Geoscience Union Meeting 2022,* SVC31-17.

Bryan, S.E., Cook, A., Evans, J.P., Colls, P.W., Wells, M.G., Lawrence, M.G., Jell, J.S., Greig, A., & Leslie, R. (2004). Pumice rafting and faunal dispersion during 2001–2002 in the Southwest Pacific: record of a dacitic submarine explosive eruption from Tonga. *Earth Planet. Sci. Lett.*, 227, 135-154.

Bryan, S.E., Cook, A.G., Evans, J.P., Hebden, K., Hurrey, L., Colls, P., Jell, J.S., Weatherly, D., and Firn, J. (2012) Rapid, long-distance dispersal by pumice rafting. (2012) *Plos one*, 7, e40583.

Coombs, M. L., Eichelberger, J. C., & Rutherford, M. J. (2003). Experimental and textural

321 constraints on mafic enclave formation in volcanic rocks. *J. Volcanol. Geothermal Res.*,
322 119, 125-144.
323 Fujiwara, T., Imai, K., Obayashi, M., Yoshida, K., Tada, N., Obana, K., Fujie, G., Ono, S, &
324 Kodaira, S. (2024). The Sofu Seamount submarine volcano present in the source area of
325 the October 2023 earthquakes and tsunamis in Japan. *Geophys. Res. Lett.*, 51(19),
326 e2024GL109766. https://doi.org/10.1029/2024GL109766
327 Earthquake Research Institute, U. Tokyo (2024) [Analysis Result] Whole rock chemical
328 composition of drifting pumice collected near Izu-Torishima and Sofugan. (in Japanese,
329 title is translated by the authors) https://www.eri.u-tokyo.ac.jp/eq/20272/
330 Grebennikov, A.V. & Maksimov, S.O. (2006) Fayalite rhyolites and a zoned magma chamber
331 of the Paleocene Yakutinskaya volcanic depression in Primorye, Russia. *J. Mineral. Petrol.*
332 *Sci.*, 101, 69-88.
333 Hiramine, R., Aoki, K., Ishimura, D., & Suzuki, T. (2023). Characteristics of drift pumice clasts
334 along the coast of the Japanese Islands: The AT tephra, representative source of drift
335 pumice clasts. *Geograph. Rep. Tokyo Metropolitan Univ.*, 58, 87-94.
336 Ishimura, D., Hiramine, R. Dispersion, fragmentation, abrasion, and organism attachment of
337 drift pumice from the 2021 Fukutoku-Oka-no-Ba eruption in Japan. *Prog. Earth Planet.*
338 *Sci.* **12**, 5 (2025). https://doi.org/10.1186/s40645-024-00678-z
339 Japan Agency for Marine-Earth Science and Technology (2024) Petrographic characteristics
340 and drift simulation study for the pumice derived from Ioto, the Ogasawara Islands, which
341 drifted to the Nansei Islands and Kanto region. (in Japanese, title is translated by the
342 authors). Accessed in 1 January 2025,
343 https://www.jamstec.go.jp/rimg/j/topics/20240531/pdf/20240530.pdf
344 Japan Coast Guard (2023) Floating debris in the sea around Torishima Island (observed on
345 October 20). (in Japanese, title is translated by the authors)
346 https://www.kaiho.mlit.go.jp/info/kouhou/post-1041.html.

347 Jochum, K.P., Weis, U., Schwager, B., Stoll, B., Wilson, S.A., Haug, G.H., Andreae, M.O.,
348 Enzweiler, J. (2016) Reference values following ISO guidelines for frequently requested
349 rock reference materials. *Geostand. Geoanal. Res.*, 40, 333-350.
350 Kato, Y. (1988) Gray pumice drifted from Fukutoku-oka-no-ba to Ryukyu Islands. *Bull.*
351 *Volcanol. Soc. Japan Series 2*, 33, 21-30 (in Japanese).
352 Kuwatani, T., Nishikawa, H., Tanaka, Y., Watanabe H., Tada, N., Nakao, A., Tamura, Y., & Ono,
353 S. (2024) Estimating the source of floating pumice found near Torishima Island, Japan: A
354 back-tracking drift simulation approach. *PREPRINT available at ESS Open Archive*,
355 https://doi.org/10.22541/essoar.172745007.73613799/v1
356 Le Bas, M.J., Le Maitre, R.W., Streckeisen, A., & Zanettin, B. A chemical classification of
357 volcanic rocks based on the total alkali-silica diagram. *J. Petrol.*, 27, 745-750.
358 Maeno, F., Kaneko, T., Ichihara, M., Suzuki, Y. J., Yasuda, A., Nishida, K., & Ohminato, T.
359 (2022). Seawater-magma interactions sustained the high column during the 2021
360 phreatomagmatic eruption of Fukutoku-Oka-no-Ba. *Com Earth & Environ.*, 3, 260.
361 Minami, H., & Tani, K. (2024). Morphological evidence of an explosive eruption event in
362 October 2023 at Sofu Seamount in the Izu-Bonin Arc. *Marine Geol.*, 477, 107405.
363 Miwa, T., Nagai, T., Kozono, T., Nakada, S., Yasuda, A., Ozawa, T., Ueda, H., Tanada, T., &
364 Fujita, E. (2024) Petrological constraints on magma storage conditions during ongoing
365 post-caldera volcanism at Ioto volcano, Ogasawara, Japan. *PREPRINT available at*
366 *Research Square*, https://doi.org/10.21203/rs.3.rs-4543053/v1
367 Mizutani, A., & Melgar, D. (2023). Potential volcanic origin of the 2023 short-period tsunami
368 in the Izu Islands, Japan. *Seismica*, 2(2). https://doi.org/10.26443/seismica.v2i2.1160
369 Mori, S., Yamashita, H., & Goto, M. (1992) Drifted pumices from Ogasawara Arc to the coast
370 of Sagami Bay. *Bull. Hiratsuka City Museum*, 15, 1-14 (in Japanese).
371 Nagai, M., Miwa, T., Nakada, S., Sumino, H., Ueda, H., Yasuda, A., Kozono, T., Hirose, T.,
372 Minami, H., & Kobayashi, T. (2024) The eruption sequence and products of the 2023

373 eruption off the Okinahama beach, Ioto(Iwojima), Japan. *Japan Geoscience Union*
374 *Meeting 2024*, SCG54-09.
375 Nakajima, R., Miyama, T., Kitahashi, T., Isobe, N., Nagano, Y., Ikuta, T., Oguri, K., Tsuchiya,
376 M., Yoshida, T., Aoki, K., Maeda, Y., Kawamura, K., Suzukawa, M., Yamauchi, T., Ritchie,
377 H., Fujikura, K., & Yabuki, A. (2022). Plastic after an extreme storm: the typhoon-induced
378 response of micro-and mesoplastics in coastal waters. *Front. Marine Sci.*, 8, 806952.
379 Nishikawa, H., Kuwatani, T., Tada, N., & Watanabe, H.K. (2023) Simulated distributions of
380 pumice rafts in Japan following eruptions at volcanic islands and submarine volcanoes.
381 *Prog. Earth Planet. Sci.*, 10, 21.
382 Obana, K., Ito, A., Fujiwara, T., Obayashi, M., Nakamura, Y., Yoshida, K., Tada, N., Nakajima,
383 T., Matsumoto, H., Fujie, G., Tanaka, S., Ono, S., & Kodaira, S. (2025) Earthquake activity
384 in the Torishima Rift and Sofu Seamount, and its relationship to the October 2023 tsunamis
385 in Japan.
386 Ohashi, M., Kennedy, B. & Gravley, D. (2024) Nucleation delay controlling the formation of
387 mafic enclaves and banded pumice. *Contrib. Mineral. Petrol.*, 179, 102.
388 https://doi.org/10.1007/s00410-024-02180-7
389 Ohno, Y., Iguchi, A., Ijima, M., Yasumoto, K., & Suzuki, A. (2022). Coastal ecological impacts
390 from pumice rafts. *Sci. Rep.*, 12, 11187. https://doi.org/10.1038/s41598-022-14614-y
391 Oikawa, T., Ishizuka, O., Iwahashi, K., Conway, C., Yamazaki, S., and Nishihara, A. (2023)
392 Characteristics of drifted pumice collected near Torishima Island in October 2023. (in
393 Japanese) accessed in 1 January 2025,
394 https://www.gsj.jp/hazards/volcano/torishima/index.html
395 Rashidov, V. A., Pilipenko, O. V., & Petrova, V. V. (2015). Petromagnetic and microprobe
396 studies of rocks in the Sofu underwater volcanic cluster, Izu-Bonin island arc, Pacific
397 Ocean. *J. Volcanol. Seis.*, 9, 182-196. https://doi.org/10.1134/S0742046315030045
398 Sakurai, R., Nakamura, M., Okumura, S., Mujin, M., & Nakatani, T. (2024). Vapor-phase

crystallization from a hydrous silicate melt: an experimental simulation of diktytaxitic texture. *Contrib. Mineral. Petrol.*, 179, 23.

Sandanbata, O., Satake, K., Takemura, S., Watada, S., Maeda, T., & Kubota, T. (2024). Enigmatic tsunami waves amplified by repetitive source events near Sofugan volcano, Japan. *Geophys. Res. Lett.*, 51(2), e2023GL106949.

Tada, N., Nishikawa, H., Ichihara, H., Watanabe Kayama, H., Kuwatani, T. (2021) Drift of an ocean bottom electromagnetometer from the Bonin to Ryukyu Islands: estimation of the path and travel time by numerical tracking experiments. *Earth Planet. Space*, 73, 224. https://doi.org/10.1186/s40623-021-01552-8

Takeuchi, S., Ishige, K., Uesawa, S., & Suwa, Y. (2024). Unsinkable, long-drifting, millimeter-sized pumice of the 2021 eruption of Fukutoku-Oka-no-Ba submarine volcano. *Prog. Earth Planet. Sci.*, 11, 47. https://doi.org/10.1186/s40645-024-00652-9

Tamura, Y., Gill, J. B., Tollstrup, D., Kawabata, H., Shukuno, H., Chang, Q., Miyazaki, T., Takahashi, T., Hirahra, Y., Kodaira, S., Ishizuka, O., Suzuki, T., Kido, Y., Fiske, R. S., & Tatsumi, Y. (2009) Silicic magmas in the Izu–Bonin Oceanic Arc and implications for crustal evolution. *J. Petrol.*, 50, 685-723.

Tamura, Y., Sato, T., Ishizuka, O., McIntosh, I., Yoshida, K., & Maeno, F. (2023) Magma genesis and interaction at Nishinoshima volcano in the Ogasawara arc: new insights from submarine deposits of the explosive 2020 eruptions. *Front. Earth Sci.*, 11:1137416. https://doi.org/10.3389/feart.2023.1137416.

Tani, K., Kawabata, H., Chang, Q., Sato, K., & Tatsumi, Y. (2005) Quantitative analyses of silicate rock major and trace elements by X-ray fluorescence spectrometer: Evaluation of analytical precision and sample preparation. *Frontier Research on Earth Evolution: IFREE Report for 2003-2004 vol. 2*.

Yoshida, K., Tamura, Y., Sato, T., Hanyu, T., Usui, Y., Chang, Q., & Ono, S. (2022a) Variety of the drift pumice clasts from the 2021 Fukutoku-Oka-no-Ba eruption, Japan. *Isl. Arc*, 31,

e12441. https://doi.org/10.1111/iar.12441

Yoshida, K., Tamura, Y., Sato, T., Sangmanee, C., Puttapreecha, R., & Ono, S. (2022b) Petrographic characteristics in the pumice clast deposited along the Gulf of Thailand, drifted from Fukutoku-Oka-no-Ba. *Geochem. J.*, 56(5), 134-137. https://doi.org/10.2343/geochemj.GJ22011

Yoshida, K., Maruya, Y., & Kuwatani, T. (2022c) Chocolate-chip cookie-like pumice from the 2021 Fukutoku-Oka-no-Ba eruption: views from SNS-related geology. Japanese Magazine of Mineralogical and Petrological Sciences, 51, 220412. (in Japanese with English abstract) https://doi.org/10.2465/gkk.220412

Yoshida, K., Miyake, A., Okumura, S.H., Ishibashi, H., Okumura, S., Okamoto, A., Niwa, Y., Kimura, M., Sato, T., Tamura, Y., & Ono, S. (2023) Oxidation-induced nanolite crystallization triggered the 2021 eruption of Fukutoku-Oka-no-Ba, Japan. Scientific Reports, 13, 7117. https://doi.org/10.1038/s41598-023-34301-w

439 Tables

440

441 Table 1. Summary of the collected samples.

Sample name	Locality	Longitude (E)	Latitude (N)	Collected date	Mineral assemblage						
					Cpx	Opx	Ol	Pl	Qz	Opaque	Frothy Patch
NC24-7	Okinawa	128.3162	26.8071	Sept. 18, 2024	+	+	b	+		Mag	exist
KTK-7	Hahajima	142.1431	26.6983	July 22, 2024	+	+	b	+		Mag	exist
OMT-3	Hahajima	142.1766	26.6241	July 22, 2024	+	+	+	+		Ilm, Mag	
HNU-1	Chichijima	142.2244	27.0816	July 21, 2024	+	+	r	+	+	Mag	
NJ24-2	Niijima	139.2550	34.3829	Oct. 8, 2024	+	+	+*	+		Mag	

442 +: appears as phenocryst. b: only in black enclave. r: only in the rind of xenocryst. *: fayalite.

443

444 Table 2. Whole rock composition of the studied pumice.

Sample	NC24-7	KTK-7	HNU-1	OMT-3	NJ24-2
	(mass%)				
SiO_2	71.86	71.97	71.25	66.93	70.19
TiO_2	0.50	0.49	0.53	0.66	0.34
Al_2O_3	14.11	14.03	14.27	15.47	14.80
Fe_2O_3	3.68	3.63	3.84	5.23	4.70
MnO	0.10	0.10	0.11	0.12	0.15
MgO	0.78	0.76	0.87	1.52	0.40
CaO	2.79	2.72	3.00	4.62	2.31
Na_2O	5.08	5.06	5.05	4.55	5.26
K_2O	1.46	1.48	1.44	1.22	2.18
P_2O_5	0.11	0.11	0.12	0.13	0.10
Total	100.46	100.36	100.46	100.45	100.43
	(mg/kg)				
Sc	6.9	7.4			
Co	4.2	4.3			
Ni	0.75	1.01			
Cu	16.45	13.64			
Rb	16.61	16.64			

Sr	109	108
Y	46.1	45.9
Cs	0.636	0.638
Ba	202	202
La	10.66	10.66
Ce	27.2	27.1
Pr	4.20	4.19
Nd	19.9	19.8
Sm	5.56	5.51
Eu	1.31	1.30
Gd	6.65	6.50
Tb	1.21	1.19
Dy	8.03	7.93
Ho	1.75	1.74
Er	5.48	5.41
Tm	0.813	0.815
Yb	5.70	5.66
Lu	0.872	0.857
Tl	0.157	0.152
Pb	4.60	4.54
Th	1.53	1.51

U	0.771	0.75

445

446 Table 3. Representative chemical composition of pyroxenes

Mineral	Clinopyroxene											Orthopyroxene							
Sample No.	NC24-7			KTK-7			HNU-1		OMT-3		NJ24-2	NC24-7		KTK-7		HNU-1	OMT-3		NJ24-2
Note	matrix	frothy	black enc.	matrix	frothy	black enc.	matrix	xenocryst	matrix	dark agg.	matrix	matrix	frothy	matrix	frothy	matrix	matrix	dark agg.	matrix
SiO_2	50.90	52.22	52.18	52.67	52.59	51.63	51.95	50.72	51.08	50.09	49.41	52.03	51.43	53.28	52.28	51.48	53.18	53.70	49.14
TiO_2	0.51	0.18	0.49	0.45	0.34	0.65	0.41	0.72	0.55	0.70	0.41	0.15	0.22	0.15	0.28	0.14	0.11	0.32	0.26
Al_2O_3	1.89	0.64	2.39	1.35	0.90	2.94	1.25	2.52	2.72	3.09	1.78	0.58	0.71	0.35	0.95	0.46	0.53	1.48	0.36
Cr_2O_3	0.00	0.05	0.08	0.00	0.01	0.00	0.04	0.05	0.01	0.00	0.04	0.03	0.05	0.00	0.00	0.02	0.04	0.01	0.00
FeO*	10.08	13.66	7.37	11.49	11.72	7.71	10.23	8.00	7.83	10.52	18.82	27.46	26.93	25.04	26.00	24.55	23.95	17.40	36.30
MnO	0.55	0.82	0.25	0.58	0.64	0.24	0.70	0.18	0.29	0.33	0.84	1.36	1.28	1.19	1.20	1.19	1.26	0.57	1.76
MgO	14.38	12.77	15.96	14.34	13.88	15.55	14.72	16.00	15.87	15.75	9.68	18.53	19.06	20.30	20.04	19.96	20.28	25.82	11.60
CaO	20.62	20.13	20.87	20.92	20.65	21.40	20.83	21.95	21.12	19.09	19.54	1.26	1.30	1.36	1.36	1.19	1.26	1.93	1.67
Na_2O	0.27	0.32	0.24	0.38	0.20	0.30	0.30	0.27	0.27	0.29	0.36	0.00	0.05	0.03	0.05	0.05	0.04	0.04	0.06
K_2O	0.00	0.00	0.01	0.00	0.03	0.00	0.01	0.00	0.01	0.00	0.01	0.00	0.00	0.00	0.00	0.00	0.02	0.03	0.01
total	99.20	100.79	99.83	102.16	100.95	100.41	100.44	100.40	99.74	99.87	100.88	#####	#####	#####	#####	99.05			#####
O	6	6	6	6	6	6	6	6	6	6	6	6	6	6	6	6	6	6	6
Si	1.91	1.96	1.92	1.93	1.96	1.90	1.93	1.86	1.89	1.86	1.89	1.96	1.94	1.98	1.94	1.96	1.99	1.93	1.95
Ti	0.01	0.01	0.01	0.01	0.01	0.02	0.01	0.02	0.02	0.02	0.01	0.00	0.01	0.00	0.01	0.00	0.00	0.01	0.01
Al	0.08	0.03	0.10	0.06	0.04	0.13	0.05	0.11	0.12	0.14	0.08	0.03	0.03	0.02	0.04	0.02	0.02	0.06	0.02
Cr	0.00	0.00	0.00	0.00	0.00	0.00	0.00	0.00	0.00	0.00	0.00	0.00	0.00	0.00	0.00	0.00	0.00	0.00	0.00

Fe^{3+}	0.08	0.06	0.03	0.09	0.04	0.07	0.09	0.15	0.10	0.13	0.14	0.04	0.08	0.02	0.07	0.04	0.00	0.07	0.07
Fe^{2+}	0.23	0.37	0.19	0.27	0.32	0.17	0.23	0.10	0.15	0.20	0.47	0.83	0.77	0.76	0.74	0.74	0.75	0.46	1.13
Mn	0.02	0.03	0.01	0.02	0.02	0.01	0.02	0.01	0.01	0.01	0.03	0.04	0.04	0.04	0.04	0.04	0.04	0.02	0.06
Mg	0.81	0.72	0.88	0.78	0.77	0.85	0.81	0.88	0.87	0.87	0.55	1.04	1.07	1.13	1.11	1.14	1.13	1.38	0.69
Ca	0.83	0.81	0.82	0.82	0.82	0.84	0.83	0.86	0.84	0.76	0.80	0.05	0.05	0.05	0.05	0.05	0.05	0.07	0.07
Na	0.02	0.02	0.02	0.03	0.01	0.02	0.02	0.02	0.02	0.02	0.03	0.00	0.00	0.00	0.00	0.00	0.00	0.00	0.00
K	0.00	0.00	0.00	0.00	0.00	0.00	0.00	0.00	0.00	0.00	0.00	0.00	0.00	0.00	0.00	0.00	0.00	0.00	0.00
X_{Mg}	0.77	0.66	0.82	0.75	0.71	0.83	0.78	0.90	0.86	0.82	0.54	0.56	0.58	0.60	0.60	0.61	0.60	0.75	0.38

Fe^{3+}/Fe^{2+} ratios were determined to have 4 cations based on 6 oxygens.

black enc.: black enclave. dark agg.: dark-colored mineral aggregate.

451 Table 4. Representative chemical composition of plagioclase

Mineral	Plagioclase												
Sample No.	NC24-7			KTK-7			HNU-1			OMT-3			NJ24-2
Note	matrix	frothy	black enc.	matrix	frothy	black enc.	core	rim	xenocryst	matrix	dark agg.	matrix	matrix
SiO_2	60.66	53.54	45.84	60.70	57.06	46.19	53.88	59.71	44.41	58.50	52.22	58.21	58.21
TiO_2	0.04	0.02	0.00	0.07	0.01	0.02	0.07	0.00	0.00	0.04	0.01	0.02	0.02
Al_2O_3	24.92	29.32	34.73	24.84	26.41	34.27	28.34	25.00	34.36	26.15	28.99	25.53	25.53
Cr_2O_3	0.01	0.02	0.08	0.07	0.00	0.00	0.04	0.02	0.02	0.03	0.00	0.02	0.02
FeO*	0.20	0.68	0.85	0.41	0.33	0.67	0.41	0.31	0.56	0.36	0.90	0.23	0.23
MnO	0.00	0.00	0.02	0.00	0.00	0.04	0.01	0.00	0.00	0.00	0.00	0.00	0
MgO	0.01	0.04	0.11	0.00	0.06	0.08	0.01	0.02	0.03	0.05	0.13	0.04	0.04
CaO	6.91	12.14	18.05	6.83	9.49	18.21	10.44	7.05	18.52	8.20	12.84	7.06	7.06
Na_2O	7.67	4.90	1.13	7.40	6.22	1.24	5.50	7.43	0.92	6.78	4.19	7.14	7.14
K_2O	0.14	0.03	0.00	0.13	0.08	0.02	0.09	0.12	0.01	0.15	0.05	0.24	0.24
total	100.55	100.70	100.82	100.46	99.67	100.75	98.78	99.67	98.83	100.27	99.34	98.50	98.50
O	8	8	8	8	8	8	8	8	8	8	8	8	8
Si	2.69	2.41	2.10	2.69	2.57	2.11	2.46	2.67	2.08	2.61	2.39	2.64	2.64
Ti	0.00	0.00	0.00	0.00	0.00	0.00	0.00	0.00	0.00	0.00	0.00	0.00	0.00
Al	1.30	1.56	1.87	1.30	1.40	1.85	1.53	1.32	1.89	1.38	1.56	1.36	1.36
Cr	0.00	0.00	0.00	0.00	0.00	0.00	0.00	0.00	0.00	0.00	0.00	0.00	0.00
Fe^{3+}	0.01	0.03	0.03	0.02	0.01	0.03	0.02	0.01	0.02	0.01	0.03	0.01	0.01
Fe^{2+}	0.00	0.00	0.00	0.00	0.00	0.00	0.00	0.00	0.00	0.00	0.00	0.00	0.00
Mn	0.00	0.00	0.00	0.00	0.00	0.00	0.00	0.00	0.00	0.00	0.00	0.00	0.00
Mg	0.00	0.00	0.01	0.00	0.00	0.01	0.00	0.00	0.00	0.00	0.01	0.00	0.00

Ca	0.33	0.59	0.88	0.32	0.46	0.89	0.51	0.34	0.93	0.39	0.63	0.34	0.34
Na	0.66	0.43	0.10	0.64	0.54	0.11	0.49	0.64	0.08	0.59	0.37	0.63	0.63
K	0.01	0.00	0.00	0.01	0.00	0.00	0.01	0.01	0.00	0.01	0.00	0.01	0.01
X_{An}	0.33	0.58	0.90	0.34	0.46	0.89	0.51	0.34	0.92	0.40	0.63	0.35	0.35

452 black enc.: black enclave. dark agg.: dark-colored mineral aggregate.

453

454

Table 5. Representative chemical composition of olivine.

Mineral	Olivine					
Sample No.	NC24-7	KTK-7	HNU-1	OMT-3		NJ24-2
Note	black enc.	black enc.	xenocryst rind	matrix	dark agg.	matrix
SiO_2	39.09	38.99	37.26	37.95	37.64	31.74
TiO_2	0.05	0.15	0.03	0.02	0.02	0.00
Al_2O_3	0.04	0.03	0.26	0.00	0.02	0.04
Cr_2O_3	0.00	0.00	0.00	0.02	0.00	0.00
FeO*	21.63	22.71	27.46	23.22	26.12	58.24
MnO	0.40	0.37	0.44	0.42	0.52	2.22
MgO	41.21	39.05	34.85	39.78	36.07	9.57
CaO	0.21	0.18	0.38	0.13	0.18	0.15
Na_2O	0.00	0.00	0.02	0.01	0.00	0.02
K_2O	0.00	0.02	0.02	0.00	0.01	0.01
total	102.62	101.49	100.71	101.55	100.58	101.97
O	4	4	4	4	4	4
Si	0.99	1.00	0.99	0.98	0.99	0.99
Ti	0.00	0.00	0.00	0.00	0.00	0.00
Al	0.00	0.00	0.01	0.00	0.00	0.00
Cr	0.00	0.00	0.00	0.00	0.00	0.00
Fe^{3+}	0.00	0.00	0.00	0.00	0.00	0.00
Fe^{2+}	0.46	0.49	0.61	0.50	0.58	1.52
Mn	0.01	0.01	0.01	0.01	0.01	0.06
Mg	1.55	1.49	1.38	1.53	1.42	0.44
Ca	0.01	0.00	0.01	0.00	0.01	0.00
Na	0.00	0.00	0.00	0.00	0.00	0.00
K	0.00	0.00	0.00	0.00	0.00	0.00
X_{Mg}	0.77	0.75	0.69	0.75	0.71	0.23

black enc.: black enclave. dark agg.: dark-colored mineral aggregate.

Table 6. Chemical composition of volcanic glass

	NC24-7	KTK-7					HNU-1			OMT-3	NJ24-2	NJ24-2
	matrix	frothy	MI in b.e.	matrix	frothy	MI in b.e.	matrix	MI in xenocryst		matrix	dark agg.	matrix
n=	5	7		10	10		9			11		10
SiO_2	77.86	76.18	63.14	77.84	76.28	62.48	76.53	64.15	76.53	76.53	74.38	72.52
TiO_2	0.24	0.18	0.26	0.23	0.29	0.36	0.21	0.32	0.29	0.29	0.35	0.28
Al_2O_3	12.13	12.49	18.60	12.23	13.09	18.65	11.97	18.15	12.49	12.49	12.52	13.88
Cr_2O_3	0.01	0.00	0.07	0.02	0.01	0.03	0.02	0.00	0.03	0.03	0.02	0.01
FeO*	1.73	1.87	3.29	1.77	2.14	2.19	1.83	1.75	2.34	2.34	3.16	3.10
MnO	0.07	0.04	0.17	0.07	0.07	0.11	0.07	0.15	0.05	0.05	0.09	0.13
MgO	0.16	0.20	0.41	0.19	0.23	0.29	0.17	0.37	0.30	0.30	0.38	0.21
CaO	1.22	1.20	6.28	1.32	1.59	5.49	1.21	4.91	1.45	1.45	1.88	1.65
Na_2O	4.33	4.43	3.90	4.29	4.55	4.32	3.91	3.78	4.26	4.26	4.23	3.88
K_2O	1.54	1.49	0.47	1.49	1.37	0.58	1.49	0.53	1.49	1.49	1.37	2.03
P_2O_5	0.02	0.02	0.22	0.03	0.04	0.25	0.03	0.19	0.03	0.03	0.20	0.03
F	0.04	0.04	0.00	0.03	0.04	0.00	0.03	0.00	0.04	0.04	0.02	0.02
Cl	0.39	0.40	0.18	0.38	0.39	0.18	0.40	0.18	0.35	0.35	0.41	0.23
total	99.72	98.54	96.98	99.90	100.10	94.91	97.86	94.49	99.65	99.65	98.99	97.98

MI: melt inclusion. b.e.: black enclave. dark agg.: dark-colored mineral aggregate.

Figure Captions

Figure 1. (a) Distribution of the sample localities investigated in this study. Representative oceanic volcanoes and major ocean currents relevant to the study area are also shown. The area indicated by the dashed box is enlarged in (b). (b) In October 2023, an earthquake swarm and related tsunamis were observed near Izu–Torishima in the Izu–Ogasawara Arc. The earthquake (T-phase) sources were determined to be located beneath the Sofu Seamount (Fujiwara et al., 2024) and, subsequently, seismic activity moved northward (Obana et al., 2025). Soon after the earthquakes, on 20 October 2023, aircraft observations identified a pumice raft of ~80 km in size near Izu–Torishima, and on 27 October, white pumice clasts that were possibly related to the raft were collected by the R/V *Keifu Maru* (white circle). A numerical simulation by Kuwatani et al. (2024) indicated the pumice raft originated from the northern area, near Sumisujima.

Figure 2. (a) The largest white pumice clasts collected on Okinawa Island in the Nansei Islands. Gray-colored blocks (frothy patches) of up to 4 cm in size are observed in the central part of the clast. (b) The same pumice clast contains black enclaves of up to 1 cm in size. The contrast is enhanced to the areas more visible. (c) A white pumice clast collected at Hahajima that also contains gray-colored frothy patches. (d–e) Other white pumice clasts collected at Chichijima and Hahajima in the Izu–Ogasawara Arc. (f) A white pumice clast collected at Niijima in the northern Izu-Ogasawara Arc.

Figure 3. (a) Total alkalis versus silica (TAS) classification diagram showing the whole-rock and glass compositions of the studied pumice samples. For comparison, data for drift pumice collected near Izu–Torishima (O23: Oikawa et al., 2023) and from the 2021 eruption of Fukutoku-Oka-no-Ba (FOB 2021, sourced from Y22a: Yoshida et al., 2022a; Y22b: Yoshida et

al., 2022b) are also shown. (b) An enlarged view of the glass analyses, showing the SiO_2-poor compositions of the frothy patches in the same samples. (c) Plot of Ba/La versus La/Sm for the selected pumice clasts (NC24-7 and KTK-7), along with data for the drift pumice collected near Izu–Torishima reported by Oikawa et al. (2023). Silicic rocks in the Izu–Ogasawara Arc (Tamura et al., 2009) and the 2021 FOB pumice are also shown for comparison.

Figure 4. (a) Backscattered electron image (BSI) showing phenocryst occurrence in pumice clast NC24-7, showing a crystal clot of Opx, Cpx, Pl, and Mag. The Pl has an antecrystic core and autocryst rim with a discontinuous boundary between the two. (b) The boundary between the ordinary matrix of the pumice and the frothy patch has a coherent coarse vesicle. (c) The Pl in a frothy patch that has an antecrystic core with a calcic composition. (d) Representative black enclave in sample NC24-7, showing an aggregate of calcic Pl, Ol, and Cpx surrounded by a microlite-rich rind. (e) Diktytaxitic cristobalite in a vesicle in the microlite-rich rind of the black enclave. (f) Melt inclusion in Cpx in the black enclave with a SiO_2 content of ~63 mass%, despite the coexistence of daughter amphibole crystals. (g) Quartz phenocryst in sample HNU-1. (i) Calcic Pl in sample HNU-1 associated with microlite-rich surrounding rind. The area indicated by the dashed orange box is enlarged in (j). (j) Microlite-rich rind around calcic Pl containing Cpx and Ol microlites. (k) Olivine and Cpx phenocrysts in the groundmass of sample OMT-3. (l) Dark-colored mineral aggregate in sample OMT-3 that consists mainly of Pl, Opx, and Cpx, along with rare Ol. (m) Iron-rich Ol associated with Pl phenocrysts, in sample NJ24-2.

511 Figures

512 Figure 1.

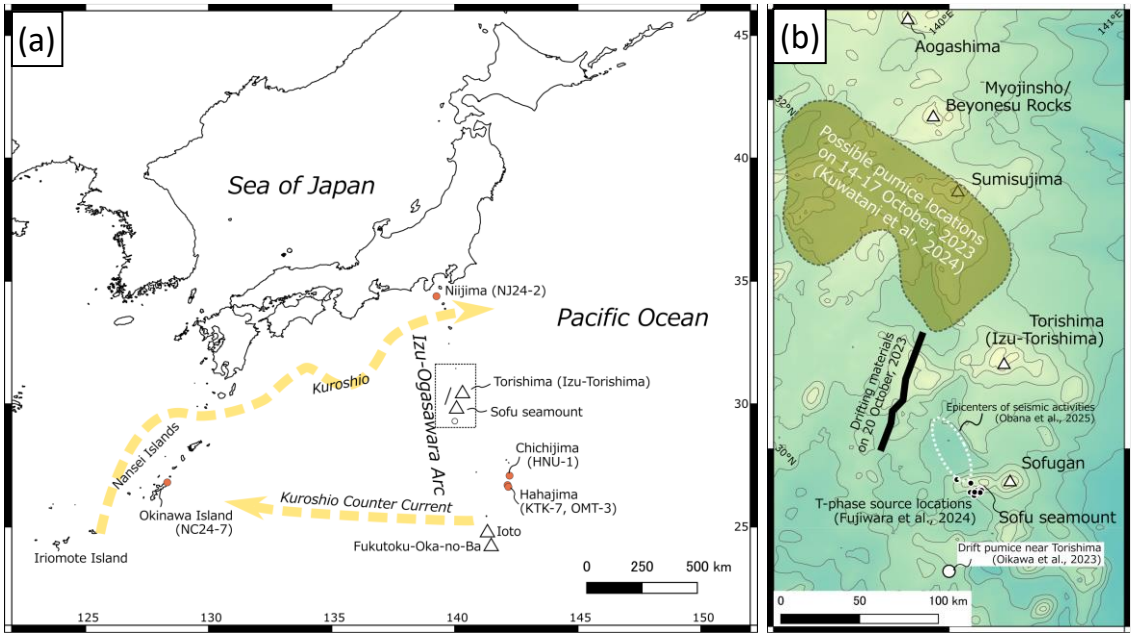

513

514

Figure 2

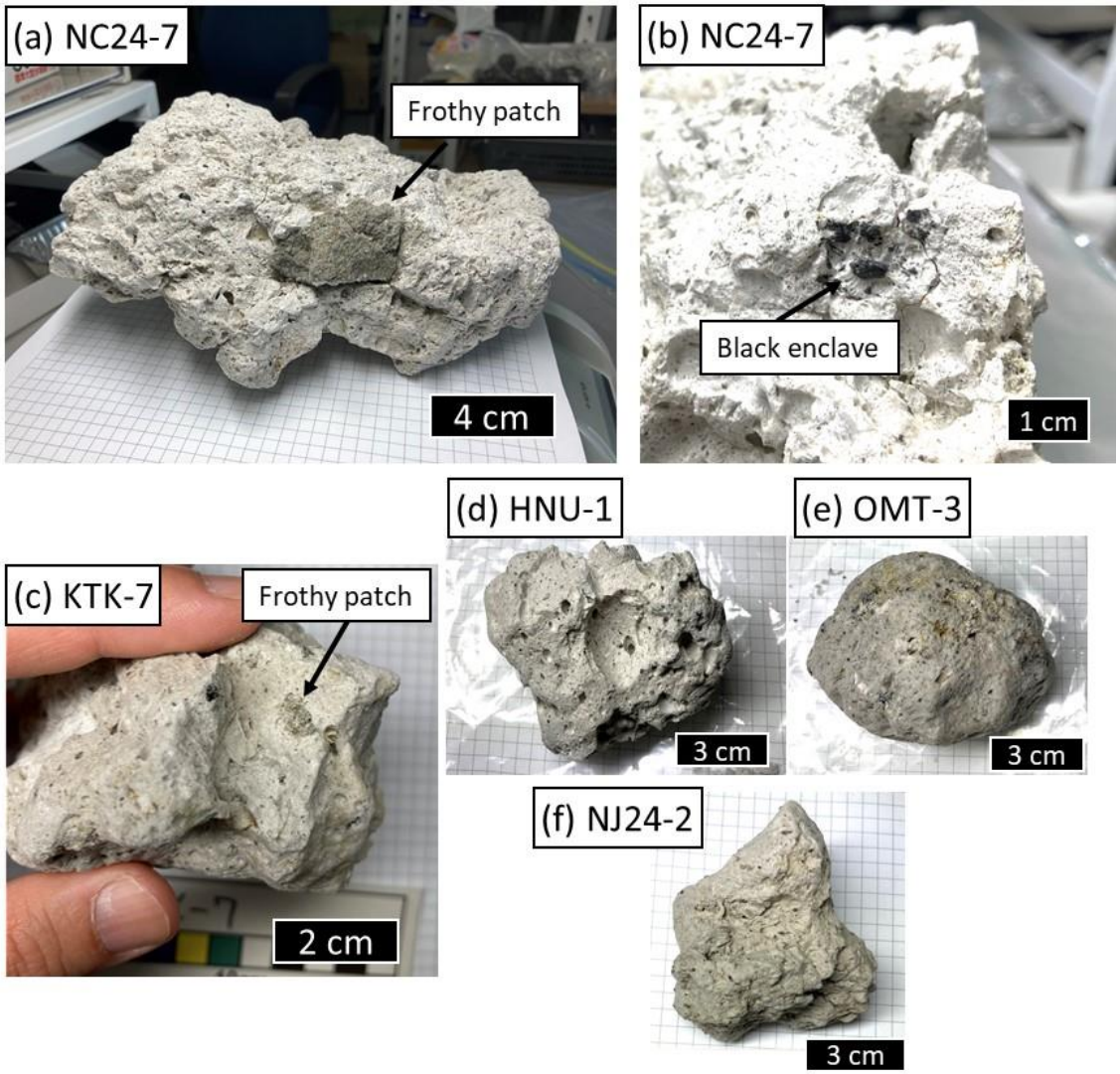
(a) NC24-7
Frothy patch
4 cm
(b) NC24-7
Black enclave
1 cm
(c) KTK-7
Frothy patch
2 cm
(d) HNU-1
3 cm
(e) OMT-3
3 cm
(f) NJ24-2
3 cm

518 Figure 3

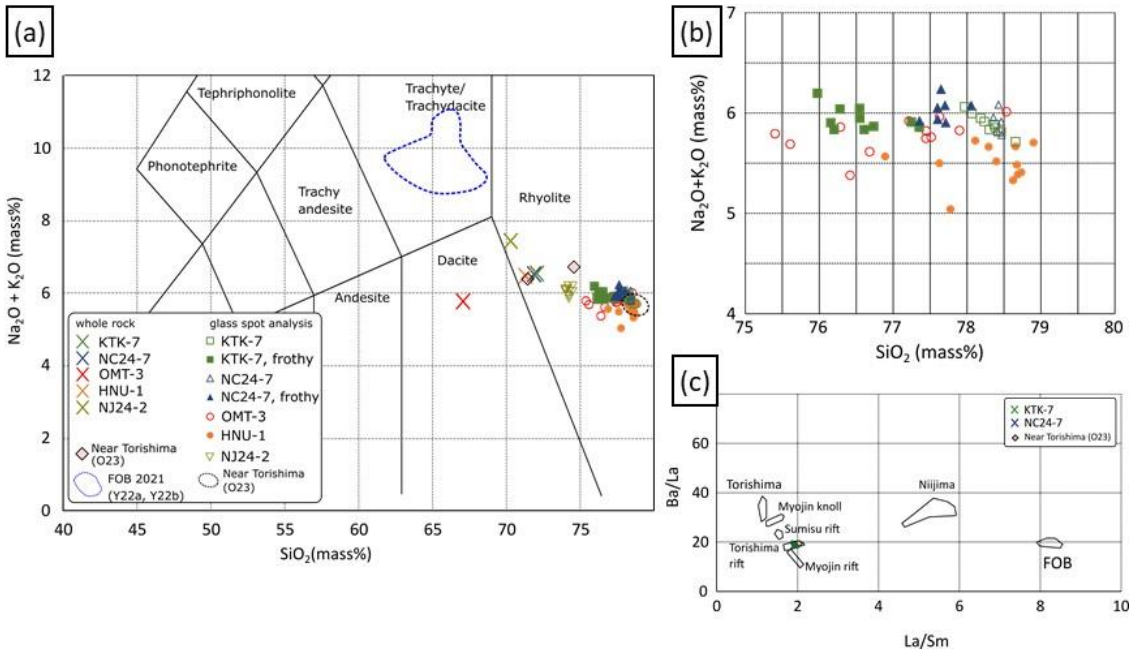

519

520

Figure 4.

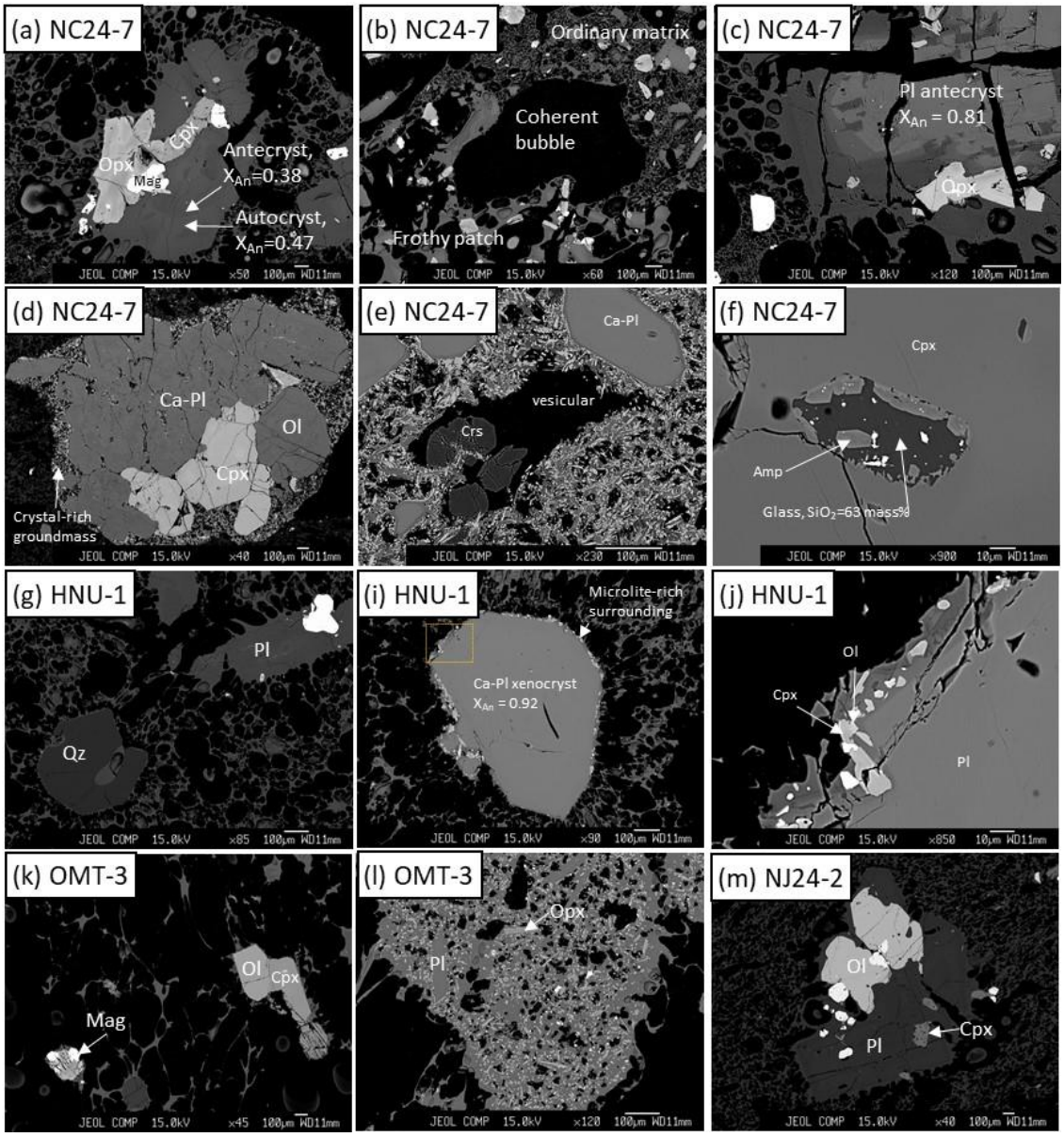
(a) NC24-7
Cpx
Opx
Mag
Antecryst, X_{An}=0.38
Autocryst, X_{An}=0.47
(b) NC24-7
Ordinary matrix
Coherent bubble
Frothy patch
(c) NC24-7
Pl antecryst X_{An} = 0.81
Opx
(d) NC24-7
Ca-Pl
Ol
Cpx
Crystal-rich groundmass
(e) NC24-7
Ca-Pl
vesicular
Crs
(f) NC24-7
Cpx
Amp
Glass, SiO_2=63 mass%
(g) HNU-1
Pl
Qz
(i) HNU-1
Microlite-rich surrounding
Ca-Pl xenocryst X_{An} = 0.92
(j) HNU-1
Ol
Cpx
Pl
(k) OMT-3
Ol
Cpx
Mag
(l) OMT-3
Opx
Pl
(m) NJ24-2
Ol
Pl
Cpx